Available online at www.sciencedirect.com
ScienceDirect
Journal of Sound and Vibration 312 (2008) 418–441
JOURNAL OF SOUND AND VIBRATION
www.elsevier.com/locate/jsvi

Numerical stability analysis for the explicit high-order finite difference analysis of rotationally symmetric shells

Troy Alvin Smith

US Army Research, Development, and Engineering Command, Aviation and Missile Research, Development, and Engineering Center, Redstone Arsenal, AL 35898, USA

Received 20 February 2006; received in revised form 26 February 2007; accepted 9 July 2007
Available online 9 January 2008

Abstract

A numerical stability analysis has been formulated to accompany the already developed explicit high-order finite difference analysis of rotationally symmetric shells subjected to time-dependent impulsive loadings. This already developed analysis utilizes a constant nodal point spacing for the spatial finite difference mesh, with the governing field differential equations formulated in terms of the transverse, meridional, and circumferential displacements as the fundamental variables. The remaining quantities which enter into the natural boundary conditions at each edge of the shell are incorporated into the complete system of equations by defining those quantities at each boundary in terms of the displacements. Surface loadings and inertia forces in each of the three displacement directions of the shell have been considered in the governing equations. Ordinary finite difference representations are used for the time derivatives. All loadings and dependent variables in the circumferential direction of the shell are expressed in Fourier series expansions. The complete system of equations is solved implicitly for the first time increment, while explicit relations are used to determine the three primary displacements within the boundary edges of the shell for the second and succeeding time increments. Separate implicit solutions at each boundary are then used to determine the remaining unspecified primary variables on and outside the boundaries. Subsequently, the remaining primary variables within the boundary edges of the shell and all secondary variables are determined explicitly. Numerical stability (or instability) of numerical solutions for given choices of spatial and time increments is determined by evaluation of the eigenvalues of the explicit coefficient matrix and comparing the maximum eigenvalue with the requirements of a stability criterion developed before by the author. Solutions for typical shells and loadings together with results of stability analyses have been included, and comparisons of the stability requirements and solutions with the requirements and solutions based upon ordinary spatial finite difference representations are included.

1. Introduction

In the absence of closed-form static or dynamic solutions for the general shell, several investigators have obtained solutions for both the static problem and the dynamic problem in which the shell is subjected to time-dependent distributed surface and thermal loadings with arbitrary time-dependent boundary conditions by numerical methods. Included in these investigators were Penny [1], who solved the symmetric bending problem of a general shell in 1961 by finite differences; Radkowski et al. [2], who solved the axisymmetric static

0022-460X/$ - see front matter © 2008 Elsevier Ltd. All rights reserved.
doi:10.1016/j.jsv.2007.07.093

Nomenclature

C_{ij}	column vector on right-hand side of Eq. (28)
E	Young's modulus
g	acceleration constant
G	coefficient matrix in equations for explicit solution for displacement variables w_n, $u_{\phi n}$, and $u_{\theta n}$
h	thickness of the shell
m_ϕ, m_θ	moments of the mechanical surface loads
M_ϕ, M_θ, $M_{\theta\phi}$	moment stress resultants
$M^0_{\phi n}$	$M_{\phi n} \times 10^{-6}$
n	integer, designating the nth Fourier component
N, Q	effective shear resultants
N^0_n, Q^0_n	$N_n \times 10^{-6}$ and $Q_n \times 10^{-6}$
N_ϕ, N_θ, $N_{\theta\phi}$	membrane stress resultants
$N^0_{\phi n}$, $M^0_{\phi n}$	$N_{\phi n} \times 10^{-6}$ and $M_{\phi n} \times 10^{-6}$
p, p_ϕ, p_θ	components of the mechanical surface loads
Q_ϕ, Q_θ	transverse shear resultants
r	distance of point on the middle surface of the shell from the axis of symmetry
R_ϕ, R_θ	principal radii of curvature of the middle surface of the shell
s	distance from an arbitrary origin along the meridian of the shell in the positive direction of ϕ
Δs	spacing between node points in the meridional finite difference mesh
t	independent time variable
Δt	increment of the time variable t
Δt(MAX)	trial value of Δt for which matrix G maximum eigenvalue is less than but nearly equal to 2
w, u_ϕ, u_θ	components of displacement of the middle surface of the shell
$\dot{w}, \dot{u}_\phi, \dot{u}_\theta$	velocities in displacement directions w, u_ϕ, and u_θ, respectively
$\ddot{w}, \ddot{u}_\phi, \ddot{u}_\theta$	accelerations in the displacement directions w, u_ϕ, and u_θ, respectively
z	distance of point on the middle surface of the shell measured from the origin along the axis of symmetry
β_θ, β_ϕ	angles of rotation of the normal to the middle surface of the shell
γ	weight of shell material per unit volume
θ, ϕ, ρ	coordinates of any point of the shell
λ	eigenvalue of the coefficient matrix G
λ_j	jth eigenvalue of the coefficient matrix G
λ(MAX)	maximum eigenvalue of the coefficient matrix G
v	Poisson's ratio

problem in 1962 by finite differences; and Budiansky and Radkowski [3], who used finite difference methods to solve the unsymmetrical static bending problem in 1963.

In 1964, Kalnins [4] also solved the static problem of rotationally symmetric shells of revolution subjected to both symmetrical and nonsymmetrical loading. Beginning with the equations of the linear classical bending theory of shells, in which the thermal effects were included, he derived a system of eight first-order ordinary differential equations which were solved by direct numerical integration over preselected segments of the shell. The resulting system of matrix equations obtained by providing continuity of the fundamental variables at the segmental division points was solved by Gaussian elimination.

The solution for the free vibration characteristics of rotationally symmetric shells with meridional variations in the shell parameters by means of his multisegment direct numerical integration approach was also obtained by Kalnins [5] in 1964. Subsequently, in 1965, the solution for the response of an arbitrary shell subjected to time-dependent surface loadings was obtained by Kraus and Kalnins [6] by means of the classical method of spectral representation. The solution was expanded in terms of the modes of free vibration as determined previously by Kalnins [5], and the orthogonality of the normal modes was proved for an arbitrary shell.

In 1965, a finite element technique for the analysis of shells of revolution under both axisymmetric and asymmetric static loading was developed by Percy et al. [7] by idealizing the shell as a series of conical frusta.

In 1966, Smith [8] published his development of procedures for the static analysis of axisymmetric shell structures under axisymmetric loading by reduction of the shell to a series of ring sections. In particular, the method may be used to analyze shells with irregular meridional geometry. Explicit expressions for influence

coefficients for each ring element are derived. Solutions are obtained by the flexibility method of indeterminate structural analysis.

In 1966, Klein [9] also published an article describing a matrix displacement finite element approach to the linear elastic analysis of multilayer shells of revolution under axisymmetric and asymmetric dynamic and impulsive loadings. The method of solution treats the shell as a series of conical frusta joined at nodal circles. Solutions are stated in the article to be numerically stable for all values of the finite difference time increment used in the step-by-step solution.

The solution for the dynamic response of a circular cylindrical shell with constant geometric and material properties and under isothermal conditions was also obtained in 1966 by Johnson and Greif [10] for the case of linear elastic shell response. These authors derived the field equations in the form of four second-order partial differential equations with respect to the meridional direction of the cylinder and obtained solutions for each Fourier harmonic by employing finite difference representations for both temporal and meridional coordinate derivatives. They obtained and compared solutions by both the implicit and the explicit methods. The numerical stability criterion for the explicit solution method given by Eq. (5.3) of Ref. [10] is empirical. It cannot therefore be assured that numerical stability, as determined by the criterion of Eq. (5.3), actually exists.

Subsequently, Smith [11,12] published reports in which he presented numerical procedures for determining the dynamic response of rotationally symmetric open-ended thin shells of revolution under time-dependent distributed impulsive and thermal loadings. Inertia forces were considered only in directions normal to the middle surface and along the meridians of the shell. The field equations were derived in the form of eight first-order partial differential equations with respect to the meridional coordinate of the shell, and the solution for each Fourier harmonic was obtained by employing low-order finite difference representations for all time and spatial derivatives. The complete system of equations was solved implicitly for the first time increment, while explicit relations were used to obtain displacements normal to the middle surface and along the meridians of the shell with the exception of quantities on and in the near vicinity of each boundary for the second and later time increments. The remaining six primary variables were then determined implicitly, while all secondary variables were subsequently found explicitly. Numerical stability (or instability) for typical shell example solutions was judged by the behavior of the solutions. No mathematical criterion for numerical stability of solutions was developed for these reports.

In 1973, Smith [13] published a report in which he presented numerical procedures for determining the dynamic response of rotationally symmetric open-ended thin shells of revolution under time-dependent surface and thermal loadings utilizing a higher-order finite difference representation of spatial derivatives than that used in Refs. [11,12]. The field equations in differential equation form were represented as in Refs. [11,12] with the exception that both surface loadings and inertia forces were considered to be acting in each of the three coordinate directions of the shell. As noted in the referenced report, initial attempts to obtain explicit solutions for the second and succeeding time increments resulted in the development of oscillatory instabilities in the numerical solutions for a considerable range of values of both spatial and time increments, including choices of impractically small values of the time increment, for all typical examples solved. Consequently, for the referenced report, the explicit solutions initially desired were abandoned in favor of a stable implicit solution to the complete system of equations for all time increments.

In 1975, Radwan and Genin [14] published their development of the equations for the determination of the nonlinear response of thin elastic shells of arbitrary geometry under either static or dynamic loading through the use of assumed, known, or calculated mode shape functions. The geometric nonlinearities were considered by employing the strain–displacement relations of the Sanders–Koiter nonlinear shell theory. The mode shape functions must satisfy the geometric boundary conditions of the shell. Their introduction into the system of governing equations leads to a system of ordinary differential equations for the generalized time coordinates. These ordinary differential equations in the time coordinates are coupled through the nonlinear terms in the equations and may for the general case be solved numerically.

In 1977, Smith [15,16] published reports in which numerical procedures were given for determining the dynamic response of rotationally symmetric open-ended thin shells of revolution under continuous time-dependent distributed surface and thermal loadings by use of both a high-order finite difference representation of the spatial derivatives and explicit relationships for the dependent variables for the second and succeeding time increments. In those reports, stable solutions were found by trial for a wide range of practical values of

both spatial and time increments by formulating the system of governing equations in terms of the transverse, meridional, and circumferential displacements only as the dependent variables in lieu of the formulation in Ref. [13], in which eight first-order differential equations with four generalized forces and four generalized displacements as the dependent variables were utilized. No mathematical criterion for numerical stability (or instability) of solutions was included in this development.

In 1983, Chang et al. [17] published their development of procedures for the linear dynamic analysis of rotationally symmetric shells using finite elements and modal expansion. Doubly curved axisymmetric shell finite elements with the loadings and displacements expanded in Fourier series in the circumferential direction of the shell and with the requisite number of frequencies and mode shapes for the meridional displacements for each Fourier number were used in the formulation of the system of equations.

In 1983, Smith [18,19] presented numerical formulations for determining both static and dynamic solutions for open-ended rotationally symmetric thin shells of revolution subjected to distributed loadings which may be discontinuous. It was shown therein that by formulating the governing system of equations in terms of the transverse, meridional, and circumferential displacements as the dependent variables and by using ordinary finite difference representations based upon a constant nodal point spacing for the derivatives in the system of equations, correct and convergent solutions are obtained without the need to segment the shell at points of discontinuous loadings. Since no mathematical criterion for numerical stability (or instability) of solutions was included in the development, values of the time increment for given values of the spatial increment to obtain stable solutions were determined by trial.

In 1991, Smith [20,21] completed development of procedures for determining the total shell response of any rotationally symmetric general shell under time-dependent (or static) surface loadings by the modal superposition method, which may be used for linearly elastic systems for which all forces applied to the structure vary with time in the same manner. The method may also be used for forces which do not vary with time in the same manner by superposition of the separate solutions for the individual time-dependent forces, but the detailed development for combining these separate solutions is not given in Refs. [20,21]. The solutions treated there are accomplished by first determining the free vibration characteristics of the shell (that is, the frequencies and mode shapes) through the use of influence coefficients for the discretized shell. These influence coefficients are evaluated by the finite difference equations for a constant nodal point spacing already developed for discontinuous distributed loadings in Ref. [18]. Subsequently, the time-dependent solution is expanded in terms of the modes of free vibration of the shell to obtain the total shell response as a summation of the several modal contributions. The surface loadings considered are the loadings p normal to the middle surface of the shell, the loadings p_ϕ along the meridian of the shell, and the loadings p_θ applied in the circumferential direction of the shell. To reduce the number of degrees of freedom of the discretized shell and thus to simplify the analysis, rotary inertia and the relatively small moments m_ϕ and m_θ due to the loadings p_ϕ and p_θ, respectively, were neglected in Ref. [20]. Thermal loadings were also not considered.

In 1994, Smith [22] published a second report in which numerical procedures were demonstrated for determining the dynamic response of rotationally symmetric open-ended thin shells of revolution under continuous time-dependent distributed surface and thermal loadings by use of both a high-order finite difference representation of the spatial derivatives and explicit expressions for the displacement variables within the boundary edges of the shell for the second and succeeding time increments. Ref. [22] constitutes a revision to Ref. [15] which involved incorporation of the equilibrium equations at the shell boundaries and which resulted in stable solutions determined by trial for either free, partially restrained, or fully restrained boundaries by use of the formulation and computer program in Ref. [22]. The spatial finite difference mesh used at the shell boundaries for Ref. [22] was also altered from that used in Ref. [15]. Additionally, for Ref. [22], the finite difference representations for the derivatives on the boundaries were altered from those used in Ref. [15] to provide a consistent order of truncation error for all derivatives. No mathematical criterion for numerical stability (or instability) of solutions was included in the development of Ref. [22].

In 1998, Smith [23,24] published his development based on the formulation of the three governing differential equations in terms of the transverse, meridional, and circumferential displacements as the fundamental variables in the field equations. The system of equations is converted to a system of ordinary spatial finite difference equations for which a variable nodal point spacing may be used together with an ordinary finite difference representation for the time derivatives. Explicit relations are obtained for the

displacements within the boundary edges of the shell for the second and succeeding time steps of computation. The references contain the development and implementation of a numerical stability (or instability) criterion based upon an eigenvalue analysis of the explicit coefficient matrices for any selected spatial finite difference mesh and time step increment. The eigenvalues and eigenvectors of the explicit coefficient matrices are found by use of an accompanying computer program subroutine EIGNCX given and described by Sellers [25].

In 2001, Smith [26] conducted a study of the effects of matrix size, the number of digits carried in the numerical calculations, and the well-conditioning (or ill-conditioning) of the matrix on the accuracy of the determined eigenvalues and eigenvectors of coefficient matrices by the subroutine EIGNCX.

In 2002, Smith [27] published the results of an extensive investigation which included the development and implementation of an eigenvalue analysis of explicit coefficient matrices to determine numerical stability (or instability) of the solution for given choices of time and spatial increments for the formulation of the shell equations based on the use of eight first-order differential equations as the field equations. It was concluded from this investigation [27] that no combination of time and spatial increments can be found for which explicit dynamic solutions are numerically stable when the finite difference equations are based upon eight first-order differential equations as the field equations and explicit relations are used for all eight fundamental variables or when explicit relations are used for the fundamental variables w_n, $u_{\phi n}$, and $\beta_{\phi n}$ only as in Refs. [11,12].

In 2004, Smith [28] incorporated into the development of Ref. [22] provision to determine by an eigenvalue analysis of the explicit coefficient matrices stability (or instability) of numerical calculations for given choices of time and spatial increments. The formulation of Ref. [22] is based upon the three displacements w_n, $u_{\phi n}$, and $u_{\theta n}$ as the fundamental variables in the field equations. Numerical solutions will be stable for this formulation if the maximum spectral radius for the coefficient matrices is less than or equal to 2. It is noted here also that the formulation of Ref. [28] is based upon the use of a constant nodal point spacing along the meridian of the shell, while the development of Ref. [23] provides for the use of any specified variable nodal point spacing along the shell meridian. Another significant difference is that the development of Ref. [28] uses high-order spatial finite difference representations, while the formulation of Ref. [23] is based upon the use of ordinary spatial finite difference representations.

It may be beneficial to indicate here in summary those references for which numerical stability (or instability) of solutions lacks a mathematical criterion and those references for which a mathematical criterion has been developed and included in the reports. No mathematical criterion for stability (or instability) has been included in Refs. [11,12,15,16,18,19,22], while a mathematical criterion for stability (or instability) of solutions based upon an eigenvalue analysis of the explicit coefficient matrices has been included for Refs. [23,24,27,28].

It has been shown in Refs. [23,24,28] that, with the governing equations formulated in terms of the transverse, meridional, and circumferential displacements as the fundamental variables and with numerical solutions found explicitly, combinations of time and spatial increments exist which result in numerically stable solutions and other combinations exist for which solutions are numerically unstable. With the use of ordinary spatial finite difference representations, the criterion for numerical stability (or instability) of solutions is given in Refs. [23,24]. The criterion for numerical stability (or instability) of solutions with a high-order finite difference representation of spatial derivatives is given in Ref. [28].

The purpose of this article is to present the development of Ref. [28] and to show comparisons of the numerical stability requirements and solutions as obtained by the formulation of Ref. [23] using ordinary spatial derivative representations and the stability requirements and solutions as found by the high-order spatial derivative representations of Ref. [28] for typical shells.

2. Governing differential equations

The development of the system of governing differential equations is based upon the linear classical theory of shells as given by Reissner [29]. The three governing differential equations are given in terms of the transverse displacement w, the meridional displacement u_ϕ, and the circumferential displacement u_θ as the unknown variables in the field equations governing the response of the shell. The remaining quantities β_ϕ, Q, N_ϕ, N, and M_ϕ, which enter into the natural boundary conditions at each rotationally symmetric edge of the shell are incorporated into the complete system of equations by defining these quantities at each boundary in

terms of the displacements w, u_ϕ, and u_θ. Four time-dependent boundary conditions may be prescribed at each boundary edge of the shell. The quantities w, u_ϕ, u_θ, β_ϕ, Q, N_ϕ, N, and M_ϕ constitute the primary variables in the system of equations. The quantities β_θ, N_θ, M_θ, Q_ϕ, $N_{\theta\phi}$, $M_{\theta\phi}$, and Q_θ constitute the secondary variables, which are found in terms of the displacements w, u_ϕ, and u_θ after solution for those displacements.

In the development of the equations, surface loadings and inertia forces in each of the displacement directions w, u_ϕ, and u_θ will be considered. The forces of rotary inertia will be neglected. The thickness h of the shell may vary between the shell boundaries and continuity of h and its derivatives through the second order is assumed. The assumption is made that $\rho/R_\phi \ll 1$ and that $\rho/R_\theta \ll 1$, where ρ is measured from the middle surface of the shell on a normal to the middle surface and is positive outward. Thus, it is assumed that $N_{\theta\phi} = N_{\phi\theta}$, and $M_{\theta\phi} = M_{\phi\theta}$. Hence, there are only five useful equations of equilibrium for a typical shell element.

All loadings and dependent variables in the circumferential direction of the shell are expressed as Fourier series expansions. Numerical solutions are obtained for each Fourier component n by use of ordinary finite difference representations for the time derivatives and high-order finite difference representations for the spatial derivatives based upon a constant nodal point spacing.

The complete system of equations is solved implicitly for the first time increment of the solution. Initial displacements and velocities are incorporated in the direction of the displacements w_n, $u_{\phi n}$, and $u_{\theta n}$ for the first time step of the solution. Explicit solutions are used to determine the three primary displacements w_n, $u_{\phi n}$, and $u_{\theta n}$ within the boundary edges of the shell for the second and later time steps, while separate implicit solutions at each boundary are used to determine the remaining unspecified primary variables on and outside the boundaries.

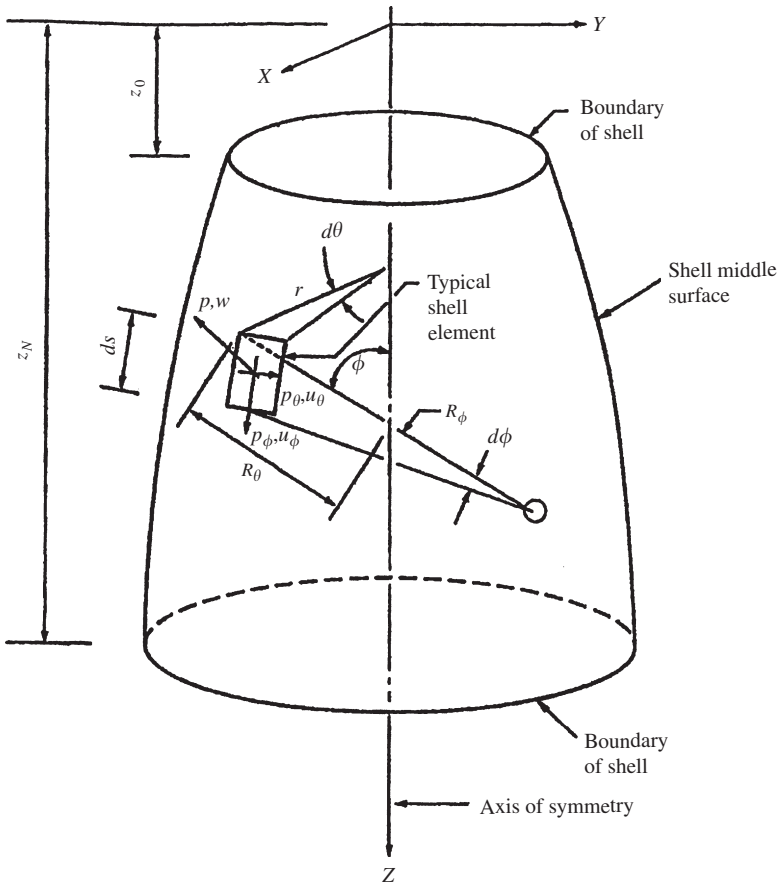

Fig. 1. Typical shell of revolution.

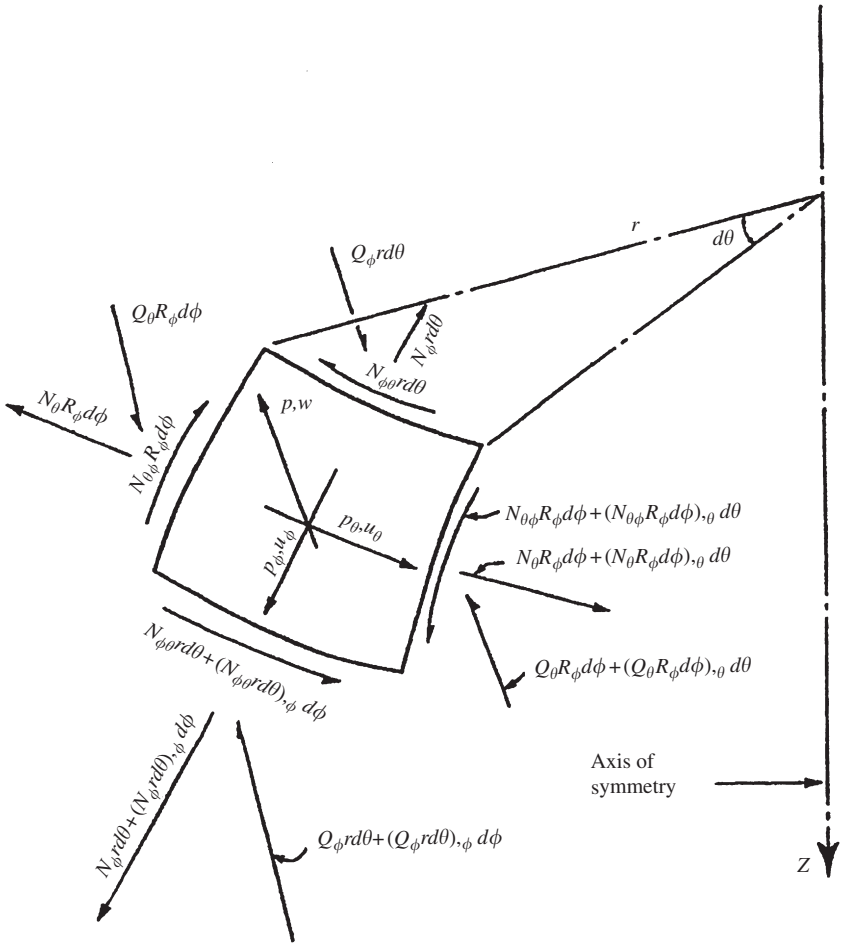

Fig. 2. Shell element membrane and shear forces.

The geometry and coordinate system for the shell's middle surface are shown in Fig. 1, shell element membrane and shear forces are given in Fig. 2, and shell element bending and twisting moments are depicted in Fig. 3. The system of differential equations described above may be found as Eqs. (1–15) in Ref. [24]. The complete development for the total system of equations involved with the subject of this article is given in Ref. [28].

3. Finite difference representation of spatial derivatives

For the finite difference representation of spatial derivatives, a high-order representation which neglects terms in the Taylor-series expansions for the derivatives containing $(\Delta s)^4$ and higher powers of Δs is used. In general, a central finite difference representation is used. The only exceptions (for which the expressions are unbalanced about the pivotal points) are for third and fourth derivatives of w_n at the boundaries s_0 and s_N; third derivatives of $u_{\phi n}$ at s_0, s_1, s_{N-1}, and s_N; first and second derivatives of $u_{\phi n}$ at s_0 and s_N; and first and second derivatives of $u_{\theta n}$ at the boundaries s_0 and s_N.

The derivatives of w are represented as

$$w_{,s}(s) = \frac{1}{\Delta s}\left[\frac{1}{12}w(s-2\Delta s) - \frac{2}{3}w(s-\Delta s) + \frac{2}{3}w(s+\Delta s) - \frac{1}{12}w(s+2\Delta s)\right], \quad (s_0 \leqslant s \leqslant s_N), \tag{1}$$

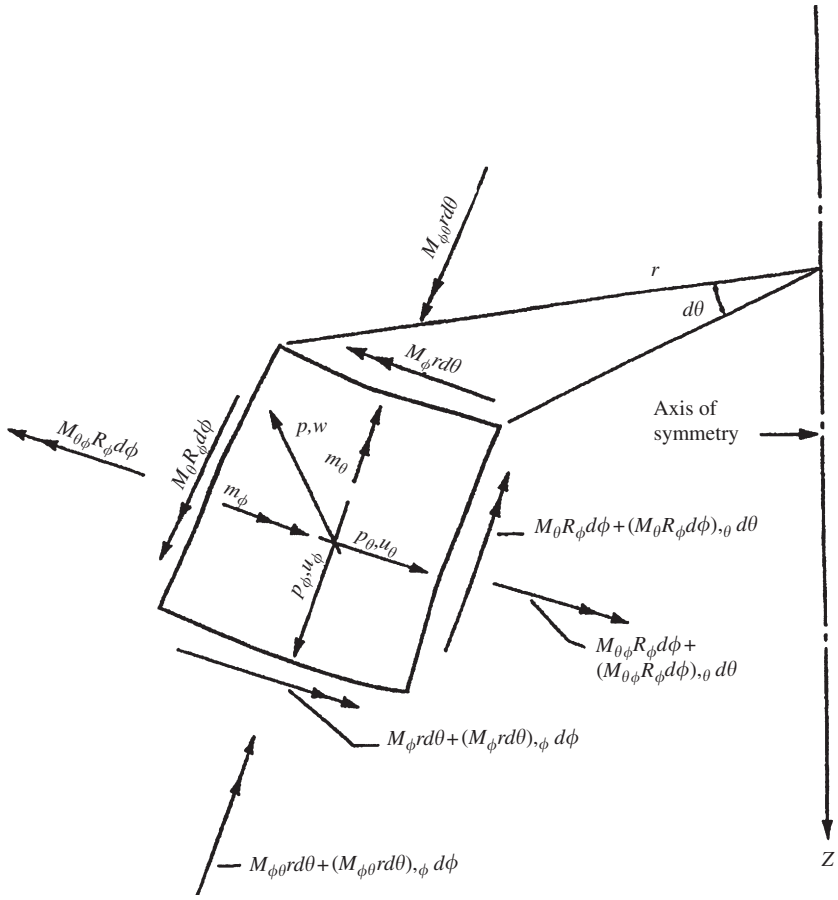

Fig. 3. Shell element bending and twisting moments.

$$w_{,ss}(s)=\frac{1}{(\Delta s)^2}\left[-\frac{1}{12}w(s-2\Delta s)+\frac{4}{3}w(s-\Delta s)-\frac{5}{2}w(s)+\frac{4}{3}w(s+\Delta s)-\frac{1}{12}w(s+2\Delta s)\right],\quad (s_0\leqslant s\leqslant s_N),\tag{2}$$

$$w_{,sss}(s)=\frac{1}{(\Delta s)^3}\left[\frac{1}{8}w(s-3\Delta s)-w(s-2\Delta s)+\frac{13}{8}w(s-\Delta s)-\frac{13}{8}w(s+\Delta s)+w(s+2\Delta s)-\frac{1}{8}w(s+3\Delta s)\right],\quad (s_1\leqslant s\leqslant s_{N-1}),\tag{3}$$

$$w_{,ssss}(s)=\frac{1}{(\Delta s)^4}\left[-\frac{1}{6}w(s-3\Delta s)+2w(s-2\Delta s)-\frac{13}{2}w(s-\Delta s)+\frac{28}{3}w(s)-\frac{13}{2}w(s+\Delta s)+2w(s+2\Delta s)-\frac{1}{6}w(s+3\Delta s)\right]\quad (s_1\leqslant s\leqslant s_{N-1}),\tag{4}$$

$$w_{,sss}(s_0)=\frac{1}{(\Delta s)^3}\left[-\frac{1}{8}w(s_{-2})-w(s_{-1})+\frac{35}{8}w(s_0)-6w(s_1)+\frac{29}{8}w(s_2)-w(s_3)+\frac{1}{8}w(s_4)\right],\tag{5}$$

$$w_{,sss}(s_N)=\frac{1}{(\Delta s)^3}\left[-\frac{1}{8}w(s_{N-4})+w(s_{N-3})-\frac{29}{8}w(s_{N-2})+6w(s_{N-1})-\frac{35}{8}w(s_N)+w(s_{N+1})+\frac{1}{8}w(s_{N+2})\right],\tag{6}$$

$$w_{,ssss}(s_0) = \frac{1}{(\Delta s)^4}\left[\frac{2}{3}w(s_{-2}) - \frac{11}{6}w(s_{-1}) + \frac{31}{6}w(s_1) - \frac{22}{3}w(s_2) + \frac{9}{2}w(s_3) - \frac{4}{3}w(s_4) + \frac{1}{6}w(s_5)\right], \tag{7}$$

$$w_{,ssss}(s_N) = \frac{1}{(\Delta s)^4}\left[\frac{1}{6}w(s_{N-5}) - \frac{4}{3}w(s_{N-4}) + \frac{9}{2}w(s_{N-3}) - \frac{22}{3}w(s_{N-2}) + \frac{31}{6}w(s_{N-1}) - \frac{11}{6}w(s_{N+1}) + \frac{2}{3}w(s_{N+2})\right]. \tag{8}$$

The derivatives of u_ϕ are given as

$$u_{\phi,s}(s) = \frac{1}{\Delta s}\left[\frac{1}{12}u_\phi(s-2\Delta s) - \frac{2}{3}u_\phi(s-\Delta s) + \frac{2}{3}u_\phi(s+\Delta s) - \frac{1}{12}u_\phi(s+2\Delta s)\right] \quad (s_1 \leqslant s \leqslant s_{N-1}), \tag{9}$$

$$u_{\phi,ss}(s) = \frac{1}{(\Delta s)^2}\left[-\frac{1}{12}u_\phi(s-2\Delta s) + \frac{4}{3}u_\phi(s-\Delta s) - \frac{5}{2}u_\phi(s) + \frac{4}{3}u_\phi(s+\Delta s) - \frac{1}{12}u_\phi(s+2\Delta s)\right], \quad (s_1 \leqslant s \leqslant s_{N-1}), \tag{10}$$

$$u_{\phi,sss}(s) = \frac{1}{(\Delta s)^3}\left[\frac{1}{8}u_\phi(s-3\Delta s) - u_\phi(s-2\Delta s) + \frac{13}{8}u_\phi(s-\Delta s) - \frac{13}{8}u_\phi(s+\Delta s) + u_\phi(s+2\Delta s) - \frac{1}{8}u_\phi(s+3\Delta s)\right] \quad (s_2 \leqslant s \leqslant s_{N-2}), \tag{11}$$

$$u_{\phi,s}(s_0) = \frac{1}{\Delta s}\left[-\frac{1}{4}u_\phi(s_{-1}) - \frac{5}{6}u_\phi(s_0) + \frac{3}{2}u_\phi(s_1) - \frac{1}{2}u_\phi(s_2) + \frac{1}{12}u_\phi(s_3)\right], \tag{12}$$

$$u_{\phi,s}(s_N) = \frac{1}{\Delta s}\left[-\frac{1}{12}u_\phi(s_{N-3}) + \frac{1}{2}u_\phi(s_{N-2}) - \frac{3}{2}u_\phi(s_{N-1}) + \frac{5}{6}u_\phi(s_N) + \frac{1}{4}u_\phi(s_{N+1})\right], \tag{13}$$

$$u_{\phi,ss}(s_0) = \frac{1}{(\Delta s)^2}\left[\frac{5}{6}u_\phi(s_{-1}) - \frac{5}{4}u_\phi(s_0) - \frac{1}{3}u_\phi(s_1) + \frac{7}{6}u_\phi(s_2) - \frac{1}{2}u_\phi(s_3) + \frac{1}{12}u_\phi(s_4)\right], \tag{14}$$

$$u_{\phi,ss}(s_N) = \frac{1}{(\Delta s)^2}\left[\frac{1}{12}u_\phi(s_{N-4}) - \frac{1}{2}u_\phi(s_{N-3}) + \frac{7}{6}u_\phi(s_{N-2}) - \frac{1}{3}u_\phi(s_{N-1}) - \frac{5}{4}u_\phi(s_N) + \frac{5}{6}u_\phi(s_{N+1})\right], \tag{15}$$

$$u_{\phi,sss}(s_0) = \frac{1}{(\Delta s)^3}\left[-\frac{15}{8}u_\phi(s_{-1}) + 7u_\phi(s_0) - \frac{83}{8}u_\phi(s_1) + 8u_\phi(s_2) - \frac{29}{8}u_\phi(s_3) + u_\phi(s_4) - \frac{1}{4}u_\phi(s_5)\right], \tag{16}$$

$$u_{\phi,sss}(s_N) = \frac{1}{(\Delta s)^3}\left[\frac{1}{8}u_\phi(s_{N-5}) - u_\phi(s_{N-4}) + \frac{29}{8}u_\phi(s_{N-3}) - 8u_\phi(s_{N-2}) + \frac{83}{8}u_\phi(s_{N-1}) - 7u_\phi(s_N) + \frac{15}{8}u_\phi(s_{N+1})\right], \tag{17}$$

$$u_{\phi,sss}(s_1) = \frac{1}{(\Delta s)^3}\left[-\frac{1}{8}u_\phi(s_{-1}) - u_\phi(s_0) + \frac{35}{8}u_\phi(s_1) - 6u_\phi(s_2) + \frac{29}{8}u_\phi(s_3) - u_\phi(s_4) + \frac{1}{8}u_\phi(s_5)\right], \tag{18}$$

$$u_{\phi,sss}(s_{N-1}) = \frac{1}{(\Delta s)^3}\left[-\frac{1}{8}u_\phi(s_{N-5}) + u_\phi(s_{N-4}) - \frac{29}{8}u_\phi(s_{N-3}) + 6u_\phi(s_{N-2}) - \frac{35}{8}u_\phi(s_{N-1}) + u_\phi(s_N) + \frac{1}{8}u_\phi(s_{N+1})\right]. \tag{19}$$

The derivatives of the variable u_θ are given by

$$u_{\theta,s}(s) = \frac{1}{\Delta s}\left[\frac{1}{12}u_\theta(s-2\Delta s) - \frac{2}{3}u_\theta(s-\Delta s) + \frac{2}{3}u_\theta(s+\Delta s) - \frac{1}{12}u_\theta(s+2\Delta s)\right] \quad (s_1 \leqslant s \leqslant s_{N-1}), \tag{20}$$

$$u_{\theta,ss}(s) = \frac{1}{(\Delta s)^2}\left[-\frac{1}{12}u_\theta(s-2\Delta s) + \frac{4}{3}u_\theta(s-\Delta s) - \frac{5}{2}u_\theta(s) + \frac{4}{3}u_\theta(s+\Delta s) - \frac{1}{12}u_\theta(s+2\Delta s)\right], \quad (s_1 \leqslant s \leqslant s_{N-1}), \tag{21}$$

$$u_{\theta,s}(s_0) = \frac{1}{\Delta s}\left[-\frac{1}{4}u_\theta(s_{-1}) - \frac{5}{6}u_\theta(s_0) + \frac{3}{2}u_\theta(s_1) - \frac{1}{2}u_\theta(s_2) + \frac{1}{12}u_\theta(s_3)\right], \tag{22}$$

$$u_{\theta,s}(s_N) = \frac{1}{\Delta s}\left[-\frac{1}{12}u_\theta(s_{N-3}) + \frac{1}{2}u_\theta(s_{N-2}) - \frac{3}{2}u_\theta(s_{N-1}) + \frac{5}{6}u_\theta(s_N) + \frac{1}{4}u_\theta(s_{N+1})\right], \tag{23}$$

$$u_{\theta,ss}(s_0) = \frac{1}{(\Delta s)^2}\left[\frac{5}{6}u_\theta(s_{-1}) - \frac{5}{4}u_\theta(s_0) - \frac{1}{3}u_\theta(s_1) + \frac{7}{6}u_\theta(s_2) - \frac{1}{2}u_\theta(s_3) + \frac{1}{2}u_\theta(s_4)\right], \tag{24}$$

$$u_{\theta,ss}(s_N) = \frac{1}{(\Delta s)^2}\left[\frac{1}{12}u_\theta(s_{N-4}) - \frac{1}{2}u_\theta(s_{N-3}) + \frac{7}{6}u_\theta(s_{N-2}) - \frac{1}{3}u_\theta(s_{N-1}) - \frac{5}{4}u_\theta(s_N) + \frac{5}{6}u_\theta(s_{N+1})\right]. \tag{25}$$

Eqs. (1)–(25), with the Fourier components of the variables in lieu of the variables as written, will be substituted as appropriate into the governing differential equations described in Section 2 of this article to make the conversion to a system of equations in spatial finite difference form.

4. Governing finite difference equations

The system of equations to be solved for each Fourier component of loading consists of Eqs. (8) of Ref. [24] applicable on the interval $s_0 \leqslant s \leqslant s_N$ and Eqs. (9) of Ref. [24] applicable at each boundary together with four additional equations prescribing four of the quantities w_n, $u_{\phi n}$, $u_{\theta n}$, $\beta_{\phi n}$, Q_n, $N_{\phi n}$, N_n, and $M_{\phi n}$ at each boundary and the equations defining the initial conditions. When this system of equations has been solved, the remaining unknown variables of the primary variables $\beta_{\phi n}$, Q_n, $N_{\phi n}$, N_n, and $M_{\phi n}$ may be found from Eqs. (9) of Ref. [24]. The secondary variables $\beta_{\theta n}$, $N_{\theta n}$, $M_{\theta n}$, $Q_{\phi n}$, $N_{\theta\phi n}$, $M_{\theta\phi n}$, and $Q_{\theta n}$ may be found on the interval $s_0 \leqslant s \leqslant s_N$ from the appropriate equations given in Ref. [28].

To solve the above system of equations, all derivatives in the equations are replaced by their finite difference equivalents to obtain a system of algebraic equations which may be applied at successive increments of the time variable. The node point layout for the spatial finite difference mesh is shown in Fig. 4, where N defines the number of equal spatial increments Δs between the boundaries s_0 and s_N. The number of equations to be solved at each time increment of the solution process is constituted by $3(N+1)$ algebraic equations in the coordinate s by writing Eqs. (8) of Ref. [24] together with Eqs. (12) of Ref. [24] at each of the N+1 meridional node points on and between the boundaries s_0 and s_N; ten equations by writing Eqs. (9) of Ref. [24] at each of the boundaries s_0 and s_N; and eight equations by prescribing four of the eight quantities w_n, $u_{\phi n}$, $u_{\theta n}$, $\beta_{\phi n}$, Q_n, $N_{\phi n}$, N_n, and $M_{\phi n}$ at each of the boundaries s_0 and s_N; thus constituting a system of $3N+21$ equations. The spatial derivatives in this system of $3N+21$ finite difference equations are defined by Eqs. (1)–(25) of this article. The time derivatives in the system of differential equations described previously have been converted to finite difference form for the first time increment by use of Eqs. (13) of Ref. [24] for the accelerations $\ddot{w}_n(s,t_1)$, $\ddot{u}_{\phi n}(s,t_1)$, and $\ddot{u}_{\theta n}(s,t_1)$ on the spatial interval $s_0 \leqslant s \leqslant s_N$; thus leading to an implicit solution to the system of $3N+21$ equations for the first time increment.

The time derivatives for the second and subsequent time increments have been represented as given by Eqs. (14) of Ref. [24] on the spatial interval $s_1 \leqslant s \leqslant s_N$. This leads to an explicit solution for the variables $w_n(s,t)$, $u_{\phi n}(s,t)$, and $u_{\theta n}(s,t)$ on the interval $s_1 \leqslant s \leqslant s_{N-1}$.

Following the explicit solution for the displacement variables on the interval $s_1 \leqslant s \leqslant s_{N-1}$, 12 variables on and adjacent to each boundary remain to be determined separately and implicitly at each boundary. For these separate implicit solutions, the accelerations $\ddot{w}_n(s_0,t)$, $\ddot{u}_{\phi n}(s_0,t)$, $\ddot{u}_{\theta n}(s_0,t)$, $\ddot{w}_n(s_N,t)$, $\ddot{u}_{\phi n}(s_N,t)$, and $\ddot{u}_{\theta n}(s_N,t)$ have been represented as given by Eqs. (15) of Ref. [24].

In order to produce better-conditioned matrices in the system of $3N+21$ finite difference equations, the force variables $N_{\phi n}$, $M_{\phi n}$, N_n, and Q_n have been transformed to the force variables $N^0_{\phi n}$, $M^0_{\phi n}$, N^0_n, and Q^0_n in

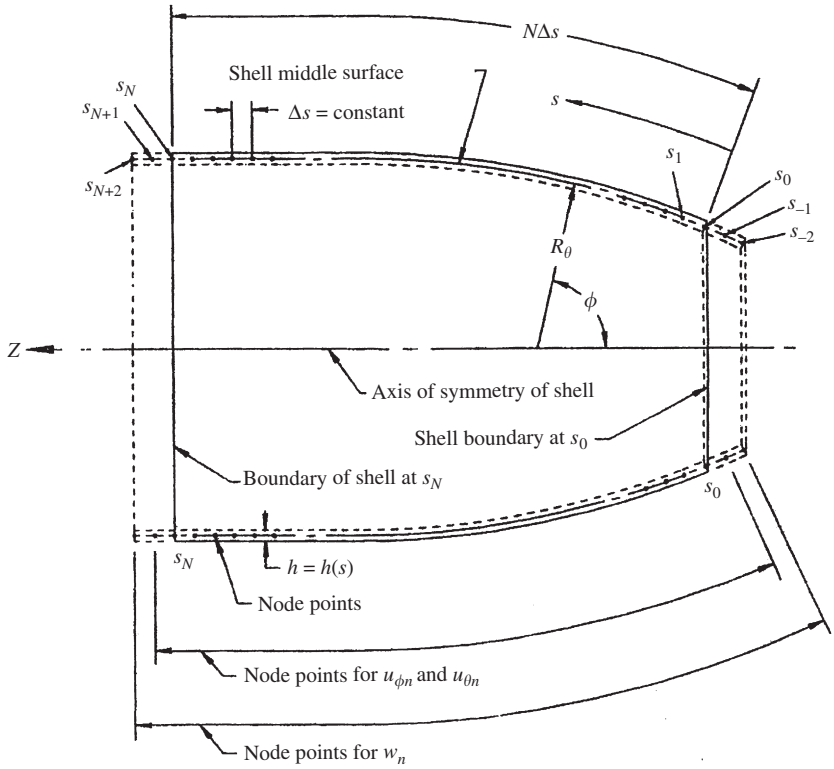

Fig. 4. Node point layout for discretized shell. N = number of equal spaces between boundaries S_0 and S_N.

accordance with Eqs. (24) of Ref. [24]. The accompanying force variable coefficients have been modified accordingly as given in Eqs. (25) of Ref. [24].

The finite difference equations for the system of $3N+21$ equations for both the time t_1 and the times $t \geqslant t_0 + 2\Delta t$ together with the computer program for obtaining the solutions may be found in Ref. [28]. This system of equations may be used to obtain solutions for static loadings by setting Δt equal to infinity in the input data and solving the system of equations for only the first time increment.

5. Selection of meridional and time increments

To obtain solutions to the system of finite difference equations described hereinbefore, choices must be made for the spatial increment Δs and the time increment Δt. For cases of static solutions, stability of numerical solutions is divorced from consideration of the choice of the meridional increment Δs. It is therefore only necessary to choose the meridional increment Δs to minimize truncation and roundoff errors. Roundoff errors will be significant as Δs approaches zero, and truncation errors will become significant as Δs is increased to values sufficiently large. Upon the basis of static solutions obtained for typical shells, it appears that static solutions obtained by use of the high-order spatial finite difference representations used in this article are sufficiently accurate if Δs is chosen to be as high as on the order of 4–6 times the thickness h of the shell [28].

For cases of dynamic solutions, it is expected that for any given choice of Δs some value of Δt(MAX) can be found for which $\Delta t \leqslant \Delta t$(MAX) will yield numerically stable solutions and for which $\Delta t > \Delta t$(MAX) will generate numerically unstable solutions. The value of Δt(MAX) will be determined by evaluating the eigenvalues of the coefficient matrix G of the displacements $w_n(s,t-\Delta t)$, $u_{\phi n}(s,t-\Delta t)$, and $u_{\theta n}(s,t-\Delta t)$ in the explicit matrix equation for $w_n(s,t)$, $u_{\phi n}(s,t)$, and $u_{\theta n}(s,t)$ on the interval $s_1 \leqslant s \leqslant s_{N-1}$ for trial values of Δt. The rather lengthy explicit equations from which the elements g_{ij} of matrix G are obtained may be found in Ref. [28]. It is noted here also that only the coefficients of the displacement values $w_n(s, t-\Delta t)$, $u_{\phi n}(s, t-\Delta t)$, and $u_{\theta n}(s, t-\Delta t)$ constitute the elements g_{ij} of matrix G. An initial trial value for Δt based upon empirical

studies given in Ref. [22] may be found from the empirical relations

$$\Delta t = (4.545\Delta s - 0.194)10^{-6} \quad (0.0625 \leqslant \Delta s \leqslant 0.1250), \tag{26a}$$

$$\Delta t = (6.491\Delta s - 0.437)10^{-6} \quad (0.1250 \leqslant \Delta s \leqslant 0.1610), \tag{26b}$$

$$\Delta t = (4.077\Delta s - 0.048)10^{-6} \quad (0.1610 \leqslant \Delta s \leqslant 0.2500), \tag{26c}$$

$$\Delta t = (3.668\Delta s + 0.053)10^{-6} \quad (0.2500 \leqslant \Delta s \leqslant 0.3220), \tag{26d}$$

$$\Delta t = (3.981\Delta s - 0.047)10^{-6} \quad (0.3220 \leqslant \Delta s \leqslant 0.5000), \tag{26e}$$

$$\Delta t = (3.787\Delta s + 0.050)10^{-6} \quad (0.5000 \leqslant \Delta s \leqslant 0.6440), \tag{26f}$$

$$\Delta t = (3.688\Delta s + 0.114)10^{-6} \quad (0.6440 \leqslant \Delta s \leqslant 0.7728), \tag{26g}$$

$$\Delta t = (3.835\Delta s)10^{-6} \quad (0.7728 \leqslant \Delta s \leqslant 0.9660). \tag{26h}$$

The development of the numerical stability criterion based upon the eigenvalues found for the coefficient matrix G is given by Eqs. (28)–(46) of Ref. [24]. This criterion is seen to be that solutions based upon the developments of this article will be numerically stable if the maximum eigenvalue of the coefficient matrix G is less than or equal to two, i.e.,

$$|\lambda(\mathrm{MAX})| \leqslant 2. \tag{27}$$

The development of the stability criterion given by Eq. (27) as shown in Ref. [24] is directly applicable for either the symmetric or the antisymmetric Fourier component with $n \geqslant 1$. Separate developments for the symmetric and antisymmetric Fourier components for $n = 0$ result in the same stability criterion [28].

It is noted that the elements g_{ij} of matrix G are functions of Δs and Δt. However, each of the elements g_{ii} along the diagonal of the matrix has an additive constant 2.0 for the displacement terms $w_n(s_j,\ t-\Delta t)$, $u_{\phi n}(s_j,\ t-\Delta t)$, and $u_{\theta n}(s_j,\ t-\Delta t)$.

For any chosen Δs, some value of Δt will be found for which $|\lambda(\mathrm{MAX})|$ is equal to 2. Solutions will also be stable as Δt is reduced, in which case, the elements g_{ij} off the diagonal are reduced in absolute value; and, similarly, the elements g_{ii} on the diagonal are altered in value. As Δt approaches zero, only the elements g_{ii} along the diagonal will be significant at a value of 2, and all eigenvalues of the matrix G will be equal to 2. As Δt is increased beyond the value Δt for which $|\lambda(\mathrm{MAX})| = 2$, the elements g_{ij} of matrix G will increase in value and produce values for $|\lambda(\mathrm{MAX})| > 2$, indicating unstable solutions.

In the solution of Eq. (38) of Ref. [24] for the eigenvalues λ_j and eigenvectors V_j by the subroutine EIGNCX, it is realized that there will be some numerical error dependent upon the number of digits carried in the calculations, the degree to which the matrix G is well-conditioned (or ill-conditioned), and the dimensions of the matrix G [26]. The accuracy of the eigenvalues and eigenvectors is expected to be diminished with increase in size of the matrix G. To measure the accuracy of the determined eigenvalues $\bar{\lambda}_j$ and eigenvectors $\bar{V}_j$, these determined quantities may be substituted into Eq. (37) of Ref. [24] to obtain

$$(G - \bar{\lambda}_j I)\bar{V}_j = C_{ij}, \tag{28}$$

where C_{ij} is a column vector representing the departure of each and every row of Eq. (28) from absolute zero. The bars over λ_j and V_j have here been used to distinguish the calculated quantities by the subroutine EIGNCX from the undetermined correct values which would satisfy Eq. (37) of Ref. [24] exactly, with absolute zero on the right-hand sides of the equations to the number of digits carried in the calculations, thus making Eq. (37) of Ref. [24] truly homogeneous.

The calculated quantities C_{ij} in Eq. (28) will be a measure of the likely error in the determination of λ_j and V_j from the subroutine EIGNCX included in Appendix B of Ref. [28]. Included in the subroutine STABIL in Appendix B of Ref. [28] is a calculation of the right-hand side of Eq. (28) so that a measure of the error in the calculated eigenvalues and eigenvectors may be available for evaluation.

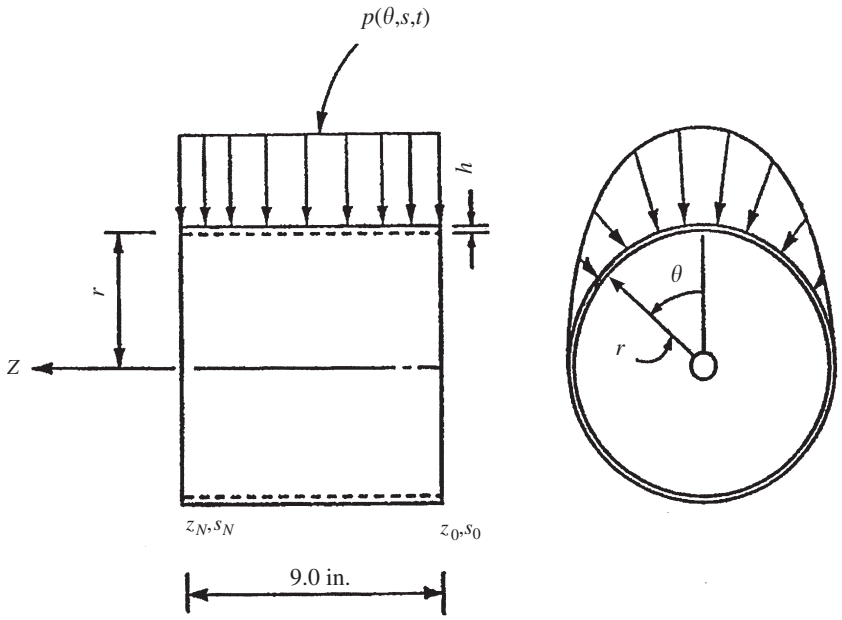

Fig. 5. Example cylindrical shell with continuous loading. The loading $p(\theta, s, t) = -1000\cos\theta(-\pi/2 \leqslant \theta \leqslant \pi/2)$. The thickness $h = 0.25$ in. The radius $r = 8.0$ in. The boundary conditions at s_0 are $w = 0$, $u_\phi = 0$, $u_\theta = 0$, and $M_\phi = 0$. The boundary conditions at s_N are $w = 0$, $u_\theta = 0$, $N_\phi = 0$, and $M_\phi = 0$.

To implement the application of the above-described development to determine numerical stability limits for the analysis of general shells, there has been included in the program in Appendix B of Ref. [28] the subroutine EIGNCX (together with the calling subroutine STABIL), which will determine all real and imaginary (if any) eigenvalues λ_j and the eigenvectors associated with the real matrix G. To demonstrate the operation and usefulness of the subroutine EIGNCX, the computer program in Appendix B of Ref. [28] will be utilized to determine by eigenvalue analyses the maximum time increment Δt for which investigated solutions are found to be stable and the minimum time increments for which investigated solutions are found to be unstable for four different nodal point spacings for the cylindrical shell and loading shown in Fig. 5. Subsequently, the stability conditions for the parabolic shell, loading, and boundary conditions shown in Fig. 6 will be evaluated.

For the cylindrical shell shown in Fig. 5, it is assumed that the initial conditions are zero. For the boundary conditions, it is assumed that w, u_ϕ, M_ϕ, and u_θ are zero at z_0 and that w, N_ϕ, M_ϕ, and u_θ are zero at z_N. A value for E of 30×10^6 pounds/in^2, a value for γ of 0.2835 pounds/in^3, and a value for v of 0.30 are assumed. Only the Fourier components for $n = 0$–4 are used. Thus, although they do not enter into the analysis for stability (or instability), the four nonzero components entering into any solution are $p_0 = -318.0$, $p_1 = -500.0$, $p_2 = -212.0$, and $p_4 = 42.0$ pounds/in^2. Shown in Table 1 are the results of our stability studies for four different nodal point spacings.

To investigate the stability conditions for the parabolic shell and loading shown in Fig. 6, it is assumed that the initial conditions are zero. It is assumed for the boundary conditions that w, u_ϕ, u_θ, and β_ϕ are zero at z_0 and that Q, N_ϕ, N, and M_ϕ are zero at z_N. A value of 30×10^6 pounds/in^2 for E, a value of 0.2835 pounds/in^3 for γ, and a value of 0.30 for v are assumed. For the given conditions, only the equations containing the symmetric Fourier components enter into the evaluation. Only the Fourier components for $n = 0$–8 are used, and, although they do not enter into the analysis for numerical stability (or instability), the nonzero loading components are $p_0 = -31.8$, $p_1 = -50.0$, $p_2 = -21.2$, $p_4 = 4.2$, $p_6 = -1.8$, and $p_8 = 1.0$ pounds/in^2. Shown in Table 2 are the results of our stability studies for the three different nodal point spacings for the parabolic shell.

To illustrate stability study results obtained by use of the subroutine EIGNCX, the eigenvalues λ(MAX) obtained for selected finite difference meshes and values of Δt for the example cylindrical shell of Fig. 5 as

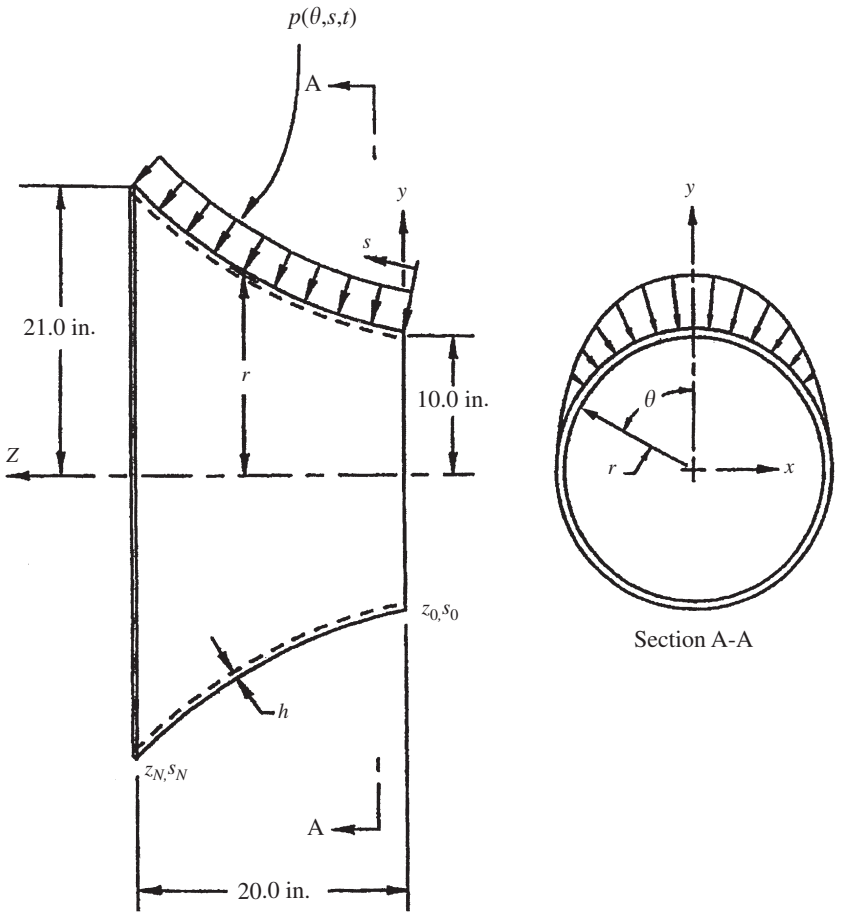

Fig. 6. Example parabolic shell with continuous loading. The loading $p(\theta,s,t) = -100\cos\theta(-\pi/2 \leqslant \theta \leqslant \pi/2)$. The radius $r = 10 + 0.15z + 0.02z^2$. The thickness $h = 0.10$ in. The boundary at s_0 is fixed against any displacement and the boundary at s_N is free of any restraint.

Table 1
Stability limits for example cylindrical shell for $n = 0$, 1, 2, and 4

Mesh spacing case no.	N no. of spaces between s_0 and s_N	Δs (in)	Time increment Δt (10^{-6} s)	
			Stable	Unstable
1	144	0.0625	$\leqslant 0.095$	$\geqslant 0.100$
2	72	0.1250	$\leqslant 0.394$	$\geqslant 0.396$
3	36	0.2500	$\leqslant 1.022$	$\geqslant 1.024$
4	18	0.5000	$\leqslant 2.048$	$\geqslant 2.050$

described previously in this section of this article are shown in Table 3. Shown in Table 4 are the eigenvalues λ(MAX) found for selected finite difference meshes and values of Δt for the example parabolic shell of Fig. 6 as also described earlier in this section of this article. It can be seen from Tables 3 and 4 that the eigenvalues λ(MAX) increase gradually as the Fourier number n increases from $n = 0$ to the maximum value of n. Thus, it is expected that stability (or instability) will be governed by the maximum value of n, which is used in the finite difference analysis. It is not therefore expected to be necessary to determine the eigenvalues for any of the Fourier components other than the maximum value of n used in the shell analysis.

Table 2
Stability limits for example parabolic shell for $n = 0$, 1, 2, 4, 6, and 8

Mesh spacing case no.	N no. of spaces between s_0 and s_N	Δs (in)	Time increment Δt (10^{-6} s)	
			Stable	Unstable
1	144	0.16100671	$\leqslant 0.640$	$\geqslant 0.660$
2	72	0.32201342	$\leqslant 1.300$	$\geqslant 1.320$
3	36	0.64402685	$\leqslant 2.620$	$\geqslant 2.640$

Table 3
Matrix G eigenvalues λ(MAX) for case numbers in Table 1

Mesh spacing case no. (Table 1)	n	Time increment Δt (10^{-6} s)	λ (MAX)	Stability condition	C_{ij} (MAX) in Eq. (28)
1	4	0.095	1.99999	Stable	0.414×10^{-11}
		0.100	2.09033	Unstable	0.150×10^{-10}
2	0	0.394	1.99989	Stable	0.541×10^{-12}
		0.396	2.00408	Unstable	0.296×10^{-10}
2	1	0.394	1.99992	Stable	0.270×10^{-11}
		0.396	2.00447	Unstable	0.229×10^{-10}
2	2	0.394	1.99995	Stable	0.245×10^{-9}
		0.396	2.00564	Unstable	0.793×10^{-11}
2	4	0.394	1.99997	Stable	0.606×10^{-12}
		0.396	2.01034	Unstable	0.183×10^{-1}
3	0	1.022	1.99926	Stable	0.102×10^{-11}
		1.024	2.00930	Unstable	0.463×10^{-9}
3	1	1.022	1.99948	Stable	0.131×10^{-11}
		1.024	2.01128	Unstable	0.146×10^{-14}
3	2	1.022	1.99970	Stable	0.348×10^{-12}
		1.024	2.01205	Unstable	0.165×10^{-9}
3	4	1.022	1.99985	Stable	0.556×10^{-12}
		1.024	2.01517	Unstable	0.426×10^{-14}
4	0	2.048	1.99705	Stable	0.109×10^{-13}
		2.050	1.99704	Stable	0.120×10^{-13}
4	1	2.048	1.99794	Stable	0.127×10^{-12}
		2.050	1.99794	Stable	0.633×10^{-12}
4	2	2.048	1.99881	Stable	0.327×10^{-12}
		2.050	1.99880	Stable	0.327×10^{-12}
4	4	2.048	1.99974	Stable	0.216×10^{-9}
		2.050	2.00756	Unstable	0.228×10^{-10}

By comparing the stability limits in Tables 1 and 2 of this article with similar results given in Tables 1 and 2 of Ref. [24] (which uses an ordinary spatial finite difference representation), it is readily seen that, for the same constant nodal point spacing, the use of a higher-order spatial finite difference representation requires a significantly smaller value of time increment Δt for stable solutions than that required for the ordinary spatial finite difference representation. This result is in accordance with expectations.

The stability limits given earlier in Tables 1 and 3 are for the cylindrical shell shown in Fig. 5, while the stability limits given in Tables 2 and 4 pertain to the parabolic shell shown in Fig. 6. These results were

Table 4
Matrix G eigenvalues λ(MAX) for case numbers in Table 2

Mesh spacing case no. (Table 2)	n	Time increment Δt (10^{-6} s)	λ(MAX)	Stability condition	C_{ij}(MAX) in Eq. (28)
1	8	0.640	1.99999	Stable	0.276×10^{-11}
		0.660	2.02878	Unstable	0.220×10^{-14}
2	0	1.300	1.99987	Stable	0.201×10^{-11}
		1.320	2.02420	Unstable	0.245×10^{-14}
2	1	1.300	1.99989	Stable	0.595×10^{-10}
		1.320	2.02456	Unstable	0.141×10^{-14}
2	2	1.300	1.99992	Stable	0.226×10^{-11}
		1.320	2.02500	Unstable	0.386×10^{-7}
2	4	1.300	1.99996	Stable	0.521×10^{-11}
		1.320	2.02680	Unstable	0.286×10^{-14}
2	6	1.300	1.99997	Stable	0.201×10^{-3}
		1.320	2.02996	Unstable	0.800×10^{-14}
2	8	1.300	1.99997	Stable	0.597×10^{-3}
		1.320	2.03472	Unstable	0.776×10^{-9}
3	0	2.620	1.99950	Stable	0.688×10^{-12}
		2.640	2.01546	Unstable	0.591×10^{-15}
3	1	2.620	1.99955	Stable	0.125×10^{-11}
		2.640	2.01782	Unstable	0.227×10^{-9}
3	2	2.620	1.99969	Stable	0.761×10^{-11}
		2.640	2.01958	Unstable	0.149×10^{-14}
3	4	2.620	1.99985	Stable	0.554×10^{-13}
		2.640	2.02683	Unstable	0.106×10^{-14}
3	6	2.620	1.99990	Stable	0.216×10^{-13}
		2.640	2.03960	Unstable	0.347×10^{-13}
3	8	2.620	1.99990	Stable	0.145×10^{-13}
		2.640	2.05889	Unstable	0.185×10^{-9}

obtained by the use of the stability criterion given by Eq. (27). It must be clear that Eq. (27) is general and is the criterion for numerical stability (or instability) of solutions for any set of shell parameters, such as the shell thickness h, Young's modulus E, Poisson's ratio v, weight of the shell material per unit volume γ, and shell geometry together with values chosen for the time increment Δt. The effects of all of these and other parameters are constituted in the numerical values of the elements g_{ij} of the explicit solution coefficient matrix G, the elements of which are evaluated in terms of these parameters.

It may be of interest here to investigate the effects of changes of the above-noted parameters on the values found for $|\lambda(\mathrm{MAX})|$ and accordingly how it affects the choice of a time increment Δt for which solutions are numerically stable for typical shells. To demonstrate this, the parabolic shell shown in Fig. 6 will be selected, and an analysis will be made of the changes in Δt required to satisfy Eq. (27) due to changes in each of the individual parameters h, E, v, γ, and shell geometry for the Fourier component $n = 8$ and $N = 36$. It is seen from Table 4 that, for the parameters used there and with $n = 8$ and $N = 36$, $|\lambda(\mathrm{MAX})| = 1.99990$ for $\Delta t = 2.620 \times 10^{-6}$ s and $|\lambda(\mathrm{MAX})| = 2.05889$ for $\Delta t = 2.640 \times 10^{-6}$ s.

For the single change from $h = 0.10$ in used for Table 4 results for $n = 8$ and $N = 36$ to $h = 0.20$ in, it is found that $|\lambda(\mathrm{MAX})| = 1.99982$ for $\Delta t = 2.620 \times 10^{-6}$ s and that $|\lambda(\mathrm{MAX})| = 2.05889$ for $\Delta t = 2.640 \times 10^{-6}$ s. Thus, in this case, doubling the value of the shell thickness h does not significantly alter $|\lambda(\mathrm{MAX})|$ and a choice of Δt, which will result in numerically stable solutions.

With a single change from $E = 30 \times 10^6$ pounds/in^2 used for Table 4 results to $E = 10 \times 10^6$ pounds/in^2, it is found that, for $n = 8$ and $N = 36$, $|\lambda(\mathrm{MAX})| = 1.99990$ for $\Delta t = 4.520 \times 10^{-6}$ s and $|\lambda(\mathrm{MAX})| = 2.00120$ for $\Delta t = 4.540 \times 10^{-6}$ s. This increase in the value of Δt for which solutions are numerically stable is in accordance with expectations for a change only in the value of E inasmuch as a second choice of Δt is the product of the square root of the ratio of the first value of E divided by the second value of E multiplied by the first value of Δt. Alternatively, if the value of E is reduced, the elements g_{ij} of the matrix G exclusive of their multiplication by $(\Delta t)^2$ are reduced in value, and this leads to a larger value of Δt for which numerically stable solutions may be found.

With the single data change from $v = 0.30$ used for Table 4 results for $n = 8$ and $N = 36$ to $v = 0.15$, the results are $|\lambda(\mathrm{MAX})| = 1.99990$ for $\Delta t = 2.700 \times 10^{-6}$ s and $|\lambda(\mathrm{MAX})| = 2.0287$ for $\Delta t = 2.720 \times 10^{-6}$ s. This increase in the value of Δt for which solutions are numerically stable with only a decrease in the value of Poisson's ratio v is expected inasmuch as it decreases the values of the elements g_{ij} exclusive of their multiplication by $(\Delta t)^2$ in the coefficient matrix G, thus resulting in an increased value of Δt for which solutions are numerically stable.

With the only data change being from $\gamma = 0.2835$ pounds/in^3 used in Table 4 results for $n = 8$ and $N = 36$ to $\gamma = 0.0954$ pounds/in^3, it is found that $|\lambda(\mathrm{MAX})| = 1.99990$ for $\Delta t = 1.52 \times 10^{-6}$ s and that $|\lambda(\mathrm{MAX})| = 2.10436$ for $\Delta t = 1.54 \times 10^{-6}$ s. These results are predictable in advance of the eigenvalue analysis for the changed value of γ inasmuch as a second choice of Δt is the product of the square root of the ratio of the second value of γ divided by the first value of γ multiplied by the first value of Δt.

To examine the effects of shell geometry on the numerical stability (or instability) requirements, the geometry shown for the parabolic shell in Fig. 6 and for which the stability (or instability) limits for $n = 8$ and $N = 36$ are shown in Table 4 will be changed to the geometry of a cylindrical shell with $r = 10$, $h = 0.10$, $\Delta s = 0.6440$ in for 36 node spacings, the boundary at s_0 fixed against any displacement, the boundary at s_N free of any restraint, and all unnamed parameters the same as given for the parabolic shell of Fig. 6. With these changes, it is found for $n = 8$ and $N = 36$ that $|\lambda(\mathrm{MAX})| = 1.99988$ for $\Delta t = 2.600 \times 10^{-6}$ s and that $|\lambda(\mathrm{MAX})| = 2.02567$ for $\Delta t = 2.620 \times 10^{-6}$ s. By comparing the eigenvalue $|\lambda(\mathrm{MAX})| = 1.99990$ for the parabolic shell as shown in Table 4 for $\Delta t = 2.620 \times 10^{-6}$ s with the eigenvalue $|\lambda(\mathrm{MAX})| = 2.02567$ for the cylindrical shell evaluated here for the same choice of $\Delta t = 2.620 \times 10^{-6}$ s, it is seen that slightly smaller values of Δt are required for the cylindrical shell than for the parabolic shell.

6. Solution results for typical shells

It is of interest to compare both static and dynamic solutions for typical shells as obtained by the use of ordinary spatial finite difference representations for the derivatives [23,24] and as found by using high-order spatial finite difference representations as described in this article [28]. In Refs. [23,24], terms of $O[(\Delta s)^2]$ and higher have been neglected in the development of the spatial finite difference expressions, while terms of $O[(\Delta s)^4]$ and higher have been neglected in the spatial representations used in this article [28]. To make these comparisons, it will be convenient to choose both the cylindrical shell of Fig. 5 and the parabolic shell of Fig. 6 for which numerical stability requirements for dynamic solutions are given in Tables 1 and 2, respectively, for the high-order spatial derivative representations of Section 3 of this article.

For the case of the cylindrical shell of Fig. 5, the boundary conditions, loadings, and material mechanical properties are as given in Section 5 of this article. Solutions at $\theta = 0$ for the static loading case as obtained by using the ordinary finite difference representations of Refs. [23,24] are shown for $u_\phi(s)$ for $\Delta s = 0.0625$, 0.1250, 0.2500, and 0.5000 in in Table 5. Solutions at $\theta = 0$ for the static loading case as obtained by using the high-order spatial derivative representations of Ref. [28] and as given in Section 3 of this article are shown for $u_\phi(s)$ for the same four values of Δs in Table 6. Solutions at $\theta = 0$ for the dynamic loading case as found by using the ordinary spatial finite difference representations of Refs. [23,24] are shown in Table 7 for $u_\phi(s, t = 0.114 \times 10^{-2}\,\mathrm{s})$ for four different combinations of Δs and Δt as given in Table 7. Dynamic loading case solutions at $\theta = 0$ as found by using the high-order finite difference representations of Ref. [28] are shown in Table 8 for $u_\phi(s, t = 0.114 \times 10^{-2}\,\mathrm{s})$ for the same four different combinations of Δs and Δt as shown in Table 8.

The boundary conditions, loadings, and material mechanical properties needed for the solutions for the parabolic shell of Fig. 6 are as given in Section 5 of this article. Solutions at $\theta = 0$ for the static loading case as

Table 5
Example cylindrical shell static solutions for $u_\phi(s)$ at $\theta = 0$ for $n = 0$, 1, 2, and 4 by ordinary finite difference method

s (in)	$u_\phi(s)$ (in) Constant nodal point spacings			
	$\Delta s = 0.0625$ in	$\Delta s = 0.1250$ in	$\Delta s = 0.2500$ in	$\Delta s = 0.5000$ in
0.00	8.0075×10^{-14}	-3.2373×10^{-15}	-3.7991×10^{-16}	-2.7799×10^{-17}
1.00	5.9292×10^{-5}	5.9210×10^{-5}	5.8873×10^{-5}	5.7350×10^{-5}
2.00	2.3733×10^{-4}	2.3706×10^{-4}	2.3600×10^{-4}	2.3160×10^{-4}
3.00	4.2662×10^{-4}	4.2625×10^{-4}	4.2477×10^{-4}	4.1874×10^{-4}
4.00	5.9505×10^{-4}	5.9468×10^{-4}	5.9320×10^{-4}	5.8716×10^{-4}
5.00	7.5612×10^{-4}	7.5579×10^{-4}	7.5446×10^{-4}	7.4901×10^{-4}
6.00	9.3506×10^{-4}	9.3472×10^{-4}	9.3336×10^{-4}	9.2779×10^{-4}
7.00	1.1455×10^{-3}	1.1451×10^{-3}	1.1432×10^{-3}	1.1358×10^{-3}
8.00	1.3554×10^{-3}	1.3547×10^{-3}	1.3521×10^{-3}	1.3414×10^{-3}
9.00	1.4554×10^{-3}	1.4546×10^{-3}	1.4514×10^{-3}	1.4387×10^{-3}

Table 6
Example cylindrical shell static solutions for $u_\phi(s)$ at $\theta = 0$ for $n = 0$, 1, 2, and 4 by high-order finite difference method

s (in)	u_ϕ (s) (in) Constant nodal point spacings			
	$\Delta s = 0.0625$ in	$\Delta s = 0.1250$ in	$\Delta s = 0.2500$ in	$\Delta s = 0.5000$ in
0.00	1.2064×10^{-14}	-5.2555×10^{-15}	-2.0244×10^{-16}	-2.1265×10^{-17}
1.00	5.9318×10^{-5}	5.9312×10^{-5}	5.9235×10^{-5}	5.8597×10^{-5}
2.00	2.3741×10^{-4}	2.3740×10^{-4}	2.3728×10^{-4}	2.3665×10^{-4}
3.00	4.2674×10^{-4}	4.2673×10^{-4}	4.2658×10^{-4}	4.2623×10^{-4}
4.00	5.9517×10^{-4}	5.9515×10^{-4}	5.9499×10^{-4}	5.9497×10^{-4}
5.00	7.5623×10^{-4}	7.5621×10^{-4}	7.5601×10^{-4}	7.5632×10^{-4}
6.00	9.3517×10^{-4}	9.3514×10^{-4}	9.3492×10^{-4}	9.3557×10^{-4}
7.00	1.1457×10^{-3}	1.1456×10^{-3}	1.1454×10^{-3}	1.1463×10^{-3}
8.00	1.3556×10^{-3}	1.3556×10^{-3}	1.3553×10^{-3}	1.3562×10^{-3}
9.00	1.4556×10^{-3}	1.4556×10^{-3}	1.4552×10^{-3}	1.4555×10^{-3}

Table 7
Example cylindrical shell dynamic solutions for u_ϕ (s, $t = 0.114 \times 10^{-2}$ s) at $\theta = 0$ for $n = 0$, 1, 2, and 4 by ordinary finite difference method

s (in)	u_ϕ (s, $t = 0.114 \times 10^{-2}$ s) Constant nodal point spacings			
	$\Delta s = 0.0625$ in, $\Delta t = 0.095 \times 10^{-6}$ s	$\Delta s = 0.1250$ in, $\Delta t = 0.380 \times 10^{-6}$ s	$\Delta s = 0.2500$ in, $\Delta t = 0.760 \times 10^{-6}$ s	$\Delta s = 0.5000$ in, $\Delta t = 1.520 \times 10^{-6}$ s
0.00	0.0000	0.0000	0.0000	0.0000
1.00	3.1233×10^{-4}	3.1225×10^{-4}	3.1325×10^{-4}	2.8864×10^{-4}
2.00	7.8792×10^{-4}	7.8605×10^{-4}	7.8362×10^{-4}	7.3425×10^{-4}
3.00	1.2148×10^{-3}	1.2115×10^{-3}	1.2019×10^{-3}	1.1613×10^{-3}
4.00	1.5242×10^{-3}	1.5226×10^{-3}	1.5122×10^{-3}	1.4837×10^{-3}
5.00	1.7780×10^{-3}	1.7768×10^{-3}	1.7682×10^{-3}	1.7258×10^{-3}
6.00	2.0416×10^{-3}	2.0383×10^{-3}	2.0281×10^{-3}	1.9914×10^{-3}
7.00	2.3677×10^{-3}	2.3640×10^{-3}	2.3450×10^{-3}	2.3179×10^{-3}
8.00	2.7020×10^{-3}	2.6982×10^{-3}	2.6775×10^{-3}	2.6352×10^{-3}
9.00	2.8577×10^{-3}	2.8541×10^{-3}	2.8380×10^{-3}	2.7808×10^{-3}

Table 8
Example cylindrical shell dynamic solutions for u_ϕ (s, $t = 0.114 \times 10^{-2}$ s) at $\theta = 0$ for $n = 0$, 1, 2, and 4 by high-order finite difference method

s (in)	u_ϕ (s, $t = 0.114 \times 10^{-2}$ s) (in) Constant nodal point spacings			
	$\Delta s = 0.0625$ in, $\Delta t = 0.095 \times 10^{-6}$ s	$\Delta s = 0.1250$ in, $\Delta t = 0.380 \times 10^{-6}$ s	$\Delta s = 0.2500$ in, $\Delta t = 0.760 \times 10^{-6}$ s	$\Delta s = 0.5000$ in, $\Delta t = 1.520 \times 10^{-6}$ s
0.00	0.0000	0.0000	0.0000	0.0000
1.00	3.1263×10^{-4}	3.1224×10^{-4}	3.1040×10^{-4}	3.0104×10^{-4}
2.00	7.8815×10^{-4}	7.8722×10^{-4}	7.8338×10^{-4}	7.6475×10^{-4}
3.00	1.2149×10^{-3}	1.2138×10^{-3}	1.2091×10^{-3}	1.1819×10^{-3}
4.00	1.5288×10^{-3}	1.5275×10^{-3}	1.5211×10^{-3}	1.4894×10^{-3}
5.00	1.7780×10^{-3}	1.7768×10^{-3}	1.7719×10^{-3}	1.7402×10^{-3}
6.00	2.0425×10^{-3}	2.0412×10^{-3}	2.0352×10^{-3}	1.9983×10^{-3}
7.00	2.3684×10^{-3}	2.3670×10^{-3}	2.3604×10^{-3}	2.3154×10^{-3}
8.00	2.7023×10^{-3}	2.7005×10^{-3}	2.6925×10^{-3}	2.6416×10^{-3}
9.00	2.8580×10^{-3}	2.8557×10^{-3}	2.8470×10^{-3}	2.7913×10^{-3}

Table 9
Example parabolic shell static solutions for u_ϕ (s) at $\theta = 0$ for $n = 0$, 1, 2, 4, 6, and 8 by ordinary finite difference method

s (in)	u_ϕ (s) (in) Constant nodal point spacings (in)		
	$\Delta s = 0.1610$ in	$\Delta s = 0.3220$ in	$\Delta s = 0.6440$ in
0.000	-7.3223×10^{-15}	2.6553×10^{-15}	2.6082×10^{-15}
2.576	3.8135×10^{-3}	3.8113×10^{-3}	3.8036×10^{-3}
5.152	5.6284×10^{-3}	5.6288×10^{-3}	5.6304×10^{-3}
7.728	5.7531×10^{-3}	5.7548×10^{-3}	5.7616×10^{-3}
10.304	4.5612×10^{-3}	4.5624×10^{-3}	4.5673×10^{-3}
12.880	2.3871×10^{-3}	2.3873×10^{-3}	2.3886×10^{-3}
15.456	-4.7450×10^{-4}	-4.7479×10^{-4}	-4.7554×10^{-4}
18.032	-3.7751×10^{-3}	-3.7754×10^{-3}	-3.7768×10^{-3}
20.608	-7.3308×10^{-3}	-7.3311×10^{-3}	-7.3330×10^{-3}
23.184	-1.1023×10^{-2}	-1.1023×10^{-2}	-1.1027×10^{-2}

found by using the ordinary finite difference representations of Refs. [23,24] are shown for $u_\phi(s)$ for $\Delta s = 0.1610$, 0.3220, and 0.6440 in in Table 9. Solutions at $\theta = 0$ for the static loading case as obtained by using the spatial derivative representations of Ref. [28] and Section 3 of this article are shown for $u_\phi(s)$ for the same three values of Δs in Table 10. Solutions at $\theta = 0$ for the dynamic loading case as found by use of the ordinary spatial finite difference representations of Refs. [23,24] are shown in Table 11 for $u_\phi(s, t = 0.720 \times 10^{-2}\,\text{s})$ for three different combinations of Δs and Δt as given in Table 11. Dynamic loading case solutions at $\theta = 0$ as found by using the high-order finite difference representations of Ref. [28] are shown in Table 12 for $u_\phi(s, t = 0.720 \times 10^{-2}\,\text{s})$ for the same three different combinations of Δs and Δt as shown in Table 12.

It is noted that for the dynamic solutions for the parabolic shell of Fig. 6 as shown in Table 11 for the ordinary spatial finite difference representations of Refs. [23,24] and as shown in Table 12 for the high-order spatial finite difference representations of Ref. [28] the choices of Δs and Δt have been selected in each case so that Δt is just below the maximum value of Δt which may be used with the chosen Δs to produce numerically stable solutions. This results in a higher truncation error for the larger values used for Δt in conjunction with the chosen Δs than the error obtained for the smaller values of Δt. To show the effects of the magnitude of Δt used for dynamic solutions for the parabolic shell of Fig. 6, solutions will be found with the use of $\Delta t = 0.30 \times 10^{-6}$ s in conjunction with all values used for Δs in obtaining these dynamic solutions. Solutions at

Table 10
Example parabolic shell static solutions for u_ϕ (s) at $\theta = 0$ for $n = 0$, 1, 2, 4, 6, and 8 by high-order finite difference method

s (in)	u_ϕ (s) (in) Constant nodal point spacings		
	$\Delta s = 0.1610$ in	$\Delta s = 0.3220$ in	$\Delta s = 0.6440$ in
0.000	8.2919×10^{-15}	7.8303×10^{-15}	2.2263×10^{-16}
2.576	3.8142×10^{-3}	3.8142×10^{-3}	3.8147×10^{-3}
5.152	5.6283×10^{-3}	5.6283×10^{-3}	5.6288×10^{-3}
7.728	5.7525×10^{-3}	5.7526×10^{-3}	5.7531×10^{-3}
10.304	4.5608×10^{-3}	4.5609×10^{-3}	4.5613×10^{-3}
12.880	2.3871×10^{-3}	2.3873×10^{-3}	2.3878×10^{-3}
15.456	-4.7428×10^{-4}	-4.7404×10^{-4}	-4.7325×10^{-4}
18.032	-3.7748×10^{-3}	-3.7745×10^{-3}	-3.7734×10^{-3}
20.608	-7.3305×10^{-3}	-7.3301×10^{-3}	-7.3287×10^{-3}
23.184	-1.1022×10^{-2}	-1.1022×10^{-2}	-1.1020×10^{-2}

Table 11
Example parabolic shell dynamic solutions for u_ϕ (s, $t = 0.720 \times 10^{-6}$ s) at $\theta = 0$ for $n = 0$, 1, 2, 4, 6, and 8 by ordinary finite difference method with Δt just below the stability limit

s (in)	u_ϕ (s, $t = 0.720 \times 10^{-6}$ s) (in) Constant nodal point spacings		
	$\Delta s = 0.1610$ in, $\Delta t = 0.60 \times 10^{-6}$ s	$\Delta s = 0.3220$ in, $\Delta t = 1.20 \times 10^{-6}$ s	$\Delta s = 0.6440$ in, $\Delta t = 2.40 \times 10^{-6}$ s
0.000	0.0000	0.0000	0.0000
2.576	5.5857×10^{-3}	5.5798×10^{-3}	5.4869×10^{-3}
5.152	8.7497×10^{-3}	8.7236×10^{-3}	8.4981×10^{-3}
7.728	9.3193×10^{-3}	9.2724×10^{-3}	8.9791×10^{-3}
10.304	7.6321×10^{-3}	7.5457×10^{-3}	7.1306×10^{-3}
12.880	4.1010×10^{-3}	3.9758×10^{-3}	3.4235×10^{-3}
15.456	-8.4112×10^{-4}	-1.0081×10^{-3}	-1.7178×10^{-3}
18.032	-6.7299×10^{-3}	-6.9055×10^{-3}	-7.6296×10^{-3}
20.608	-1.3046×10^{-2}	-1.3198×10^{-2}	-1.3845×10^{-2}
23.184	-1.9279×10^{-2}	-1.9392×10^{-2}	-1.9899×10^{-2}

Table 12
Example parabolic shell dynamic solutions for u_ϕ ($s, t = 0.720 \times 10^{-6}$ s) at $\theta = 0$ for $n = 0$, 1, 2, 4, 6, and 8 by high-order finite difference method with Δt just below the stability limit

s (in)	u_ϕ ($s, t = 0.720 \times 10^{-6}$ s) (in) Constant nodal point spacings		
	$\Delta s = 0.1610$ in, $\Delta t = 0.60 \times 10^{-6}$ s	$\Delta s = 0.3220$ in, $\Delta t = 1.20 \times 10^{-6}$ s	$\Delta s = 0.6440$ in, $\Delta t = 2.40 \times 10^{-6}$ s
0.000	0.0000	0.0000	0.0000
2.576	5.5475×10^{-3}	5.5174×10^{-3}	5.4593×10^{-3}
5.152	8.6932×10^{-3}	8.6464×10^{-3}	8.5443×10^{-3}
7.728	9.2711×10^{-3}	9.2238×10^{-3}	9.1132×10^{-3}
10.304	7.6052×10^{-3}	7.5683×10^{-3}	7.4828×10^{-3}
12.880	4.1078×10^{-3}	4.0902×10^{-3}	4.0499×10^{-3}
15.456	-7.8499×10^{-4}	-7.7173×10^{-4}	-7.4476×10^{-4}
18.032	-6.6283×10^{-3}	-6.5752×10^{-3}	-6.4575×10^{-3}
20.608	-1.2911×10^{-2}	-1.2816×10^{-2}	-1.2596×10^{-2}
23.184	-1.9101×10^{-2}	-1.8948×10^{-2}	-1.8604×10^{-2}

Table 13
Example parabolic shell dynamic solutions for u_ϕ $(s, t = 0.720 \times 10^{-6}\,\text{s})$ at $\theta = 0$ for $n = 0$, 1, 2, 4, 6, and 8 by ordinary finite difference method with $\Delta t = 0.30 \times 10^{-6}\,\text{s}$

s (in)	u_ϕ $(s, t = 0.720 \times 10^{-6}\,\text{s})$ (in) Constant nodal point spacings		
	$\Delta s = 0.1610\,\text{in}$, $\Delta t = 0.30 \times 10^{-6}\,\text{s}$	$\Delta s = 0.3220\,\text{in}$, $\Delta t = 0.30 \times 10^{-6}\,\text{s}$	$\Delta s = 0.6440\,\text{in}$, $\Delta t = 0.30 \times 10^{-6}\,\text{s}$
0.000	0.0000	0.0000	0.0000
2.576	5.5861×10^{-3}	5.5808×10^{-3}	5.4840×10^{-3}
5.152	8.7503×10^{-3}	8.7252×10^{-3}	8.4841×10^{-3}
7.728	9.3196×10^{-3}	9.2727×10^{-3}	8.9521×10^{-3}
10.304	7.6322×10^{-3}	7.5439×10^{-3}	7.0913×10^{-3}
12.880	4.1008×10^{-3}	3.9726×10^{-3}	3.3760×10^{-3}
15.456	-8.4154×10^{-4}	-1.1129×10^{-3}	-1.7742×10^{-3}
18.032	-6.7307×10^{-3}	-6.9123×10^{-3}	-7.6933×10^{-3}
20.608	-1.3048×10^{-2}	-1.3207×10^{-2}	-1.3914×10^{-2}
23.184	-1.9280×10^{-2}	-1.9399×10^{-2}	-1.9961×10^{-2}

Table 14
Example parabolic shell dynamic solutions for u_ϕ $(s, t = 0.720 \times 10^{-6}\,\text{s})$ at $\theta = 0$ for $n = 0$, 1, 2, 4, 6, and 8 by high-order finite difference method with $\Delta t = 0.30 \times 10^{-6}\,\text{s}$

s (in)	u_ϕ $(s, t = 0.720 \times 10^{-6}\,\text{s})$ (in) Constant nodal point spacings		
	$\Delta s = 0.1610\,\text{in}$, $\Delta t = 0.30 \times 10^{-6}\,\text{s}$	$\Delta s = 0.3220\,\text{in}$, $\Delta t = 0.30 \times 10^{-6}\,\text{s}$	$\Delta s = 0.6440\,\text{in}$, $\Delta t = 0.30 \times 10^{-6}\,\text{s}$
0.000	0.0000	0.0000	0.0000
2.576	5.5476×10^{-3}	5.5188×10^{-3}	5.4676×10^{-3}
5.152	8.6935×10^{-3}	8.6490×10^{-3}	8.5591×10^{-3}
7.728	9.2713×10^{-3}	9.2257×10^{-3}	9.1255×10^{-3}
10.304	7.6051×10^{-3}	7.5686×10^{-3}	7.4890×10^{-3}
12.880	4.1075×10^{-3}	4.0885×10^{-3}	4.0482×10^{-3}
15.456	-7.8558×10^{-4}	-7.7519×10^{-4}	-7.5563×10^{-4}
18.032	-6.6293×10^{-3}	-6.5805×10^{-3}	-6.4793×10^{-3}
20.608	-1.2913×10^{-2}	-1.2823×10^{-2}	-1.2628×10^{-2}
23.184	-1.9102×10^{-2}	-1.8956×10^{-2}	-1.8633×10^{-2}

$\theta = 0$ for the dynamic loading case as found with the ordinary finite difference representations of Refs. [23,24] are given in Table 13 for $u_\phi(s,\ t = 0.720 \times 10^{-2}\,\text{s})$ for three different combinations of Δs and Δt as given in Table 13. Dynamic loading case solutions at $\theta = 0$ as found by using the high-order finite difference representations of Ref. [28] are shown in Table 14 for $u_\phi(s,\ t = 0.720 \times 10^{-2}\,\text{s})$ for the same three different combinations of Δs and Δt as shown in Table 14.

Comparison of the static solution results given in Table 5 for the example cylindrical shell of Fig. 5 as found by the ordinary spatial finite difference representation of derivatives [23,24] with the results given in Table 6 as found by the high-order spatial finite difference representation of derivatives [28] shows that the ordinary finite difference results are converging toward the high-order finite difference results as the increment Δs is reduced. Thus, for the small values of Δs, the results are closely identical. It is seen also that, for the high-order spatial finite difference representation of derivatives, the static solution results are quite close for all values of Δs. Similar observations are evident when the solutions for the parabolic shell of Fig. 6 as given in Table 9 for the ordinary spatial finite difference representations [23,24] are compared with the solutions given in Table 10 for the high-order spatial finite difference representations.

It may be seen by comparing the dynamic solutions in Table 7 for the example cylindrical shell of Fig. 5 as found by the ordinary spatial finite difference representation of derivatives [23,24] with the results given in Table 8 as found by the high-order finite difference representation of derivatives [28] that the results are very

close to identical for the choice of $\Delta s = 0.0625$ in and $\Delta t = 0.095 \times 10^{-6}$ s. As the values of Δs and Δt are both increased, the degree of agreement between the results given in Tables 7 and 8 is diminished as a result of the truncation error of $O[(\Delta s)^2, (\Delta t)^2]$ for the ordinary spatial finite difference representations and the truncation error of $O[(\Delta s)^4, (\Delta t)^2]$ for the high-order spatial finite difference representations. Similar observations may be made when the solutions for the parabolic shell of Fig. 6 given in Table 11 for the ordinary spatial finite difference representations [23,24] are compared with solutions in Table 12 for the high-order spatial finite difference representations [28].

By comparing the dynamic solutions for the parabolic shell of Fig. 6 as shown in Tables 11 and 13 for the ordinary spatial finite difference representations, it is seen that the results obtained by using $\Delta s = 0.1610$ in and $\Delta t = 0.60 \times 10^{-6}$ s in Table 11 are in very good agreement with the results found by using $\Delta s = 0.1610$ in and $\Delta t = 0.30 \times 10^{-6}$ s in Table 13. This good agreement diminishes as the values used for Δs are increased. Similar observations pertain when comparisons are made between the dynamic solutions given in Tables 12 and 14 for the high-order spatial finite difference representations.

In comparing the static solutions given in Tables 5, 6, 9, and 10 with the dynamic solutions shown in Tables 7, 8, 11, 12, 13, and 14, it is seen that significantly better agreement between solutions by the ordinary and high-order spatial finite difference representations is obtained for static solutions than for dynamic solutions. Although the static solutions have a truncation error of $O[(\Delta s)^2)]$ for the ordinary spatial finite difference representations [23,24] and a truncation error of $O[(\Delta s)^4)]$ for the high-order spatial finite difference representations [28], both solutions, in the absence of significant roundoff error, converge to the exact solution as Δs is sufficiently reduced. Furthermore, the static solutions are accomplished in only one time increment of computation. Static solutions found by the high-order spatial finite difference representations are closer to the exact solutions than solutions by the ordinary spatial finite difference representations for any Δs, but they will agree for a sufficiently small value of Δs. In the case of dynamic solutions, there is a consistent truncation error of $O[(\Delta s)^4, (\Delta t)^2]$ for the high-order representations [28], while the consistent truncation error for the ordinary representations [23,24] is of $O[(\Delta s)^2, (\Delta t)^2]$. Essentially, there exist truncation errors for the dynamic solutions case, which do not exist for the static case. Additionally, for the dynamic case, there exist roundoff and truncation errors from a multiplicity of solution times as opposed to the one-time solution for the static case. Thus, it is not expected that agreement between dynamic solutions based upon ordinary and high-order representations of spatial derivatives will be as good as agreement between static solutions by the ordinary and high-order spatial finite difference representations.

7. Conclusions

The purpose of Ref. [28] was to incorporate into the development of Ref. [22] provisions to determine by eigenvalue analysis of the explicit coefficient matrices stability (or instability) of numerical solutions based upon a high-order constant nodal point spacing for spatial derivatives. A second objective was to compare the numerical stability requirements based upon the high-order constant nodal point spacing finite difference representation of spatial derivatives [28] with the requirements based upon an ordinary spatial derivative representation of spatial derivatives [23,24] for typical shells. A third objective was to compare the convergence and accuracy of solutions together with the stability requirements for the ordinary and high-order spatial finite difference representations for these typical shells.

It may be seen by examination of the stability limits given in Tables 1 and 2 (found by eigenvalue analyses of the explicit coefficient matrices) for a high-order spatial finite difference representation of the derivatives that there exist combined choices of the time increment Δt and the spatial increment Δs for which numerical solutions are stable and other combinations of these increments for which numerical solutions will be unstable. It is further seen that for given values of the spatial increment Δs the maximum time increment Δt for stable solutions for this high-order spatial finite difference representation [28] is less than the maximum time increment Δt which may be used to obtain stable solutions for an ordinary finite difference representation of spatial derivatives [23,24].

The results and observations for both static and dynamic solutions for typical shells presented in Section 6 demonstrate that larger values of both the time increment Δt and the spatial increment Δs may be used with the high-order spatial finite difference representation of spatial derivatives than with ordinary spatial finite

difference representations [23,24] to obtain stable solutions and given accuracy of solutions. It is noted also that closer convergence to the exact solution for either spatial finite difference representation may, in the absence of significant roundoff error, be obtained by sufficient reduction of the magnitude of the spatial increment Δs and, for the dynamic case, the time increment Δt. Thus, with a sufficient reduction of the spatial increment Δs and, for the dynamic case, the time increment Δt, solutions for the high-order and the ordinary spatial finite difference representations may be made to agree as closely as desired.

Acknowledgments

Grateful acknowledgment is accorded to Mr. Michael D. Parker, Systems Simulation and Development Directorate, Research, Development, and Engineering Command, Redstone Arsenal, Alabama, who implemented the author's computer program on the US Army Aviation and Missile Command Hewlett-Packard Computing System, obtained all solutions for Ref. [28] and this article on that system, and engaged in valuable discussions with the author during the program development.

The invaluable contribution of Mr. William R. Sellers Jr. (deceased), formerly an employee of the US Army Missile Command, Redstone Arsenal, Alabama, who in 1988 developed the program subroutine EIGNCX for the numerical evaluation of the real and imaginary components of the eigenvalues and eigenvectors of a general matrix is also recognized and appreciated.

References

[1] R.K. Penny, Symmetrical bending of the general shell of revolution by finite difference methods, *Journal of Mechanical Engineering Science* 3 (1961) 369–377.
[2] P.P. Radkowski, R.M. Davis, M.R. Bolduc, Numerical analysis of equations of thin shells of revolution, *ARS Journal* 32 (1962) 36–41.
[3] B. Budiansky, P.P. Radkowski, Numerical analysis of unsymmetrical bending of shells of revolution, *AIAA Journal* 1 (1963) 1833–1842.
[4] A. Kalnins, Analysis of shells of revolution subjected to symmetrical and nonsymmetrical loads, *Journal of Applied Mechanics—Transactions of the ASME 31E* 3 (1964) 467–476.
[5] A. Kalnins, Free vibration of rotationally symmetric shells, *Journal of the Acoustical Society of America* 36 (1964) 1355–1365.
[6] H. Kraus, A. Kalnins, Transient vibration of thin elastic shells, *Journal of the Acoustical Society of America* 38 (1965) 994–1002.
[7] J.H. Percy, T.H.H. Pian, S. Klein, D.R. Navaratna, Application of matrix displacement method to linear elastic analysis of shells of revolution, *AIAA Journal* 3 (1965) 2138–2145.
[8] T.A. Smith, Analysis of axisymmetric shell structures under axisymmetric loading by the finite element method, US Army Missile Command Technical Report RS-TR-66-8, Redstone Arsenal, Alabama, 1966.
[9] S. Klein, Vibrations of multi-layer shells of revolution under dynamic and impulsive loading, *Shock and Vibration Bulletin* 35 (1966) 27–44.
[10] D.E. Johnson, R. Greif, Dynamic response of a cylindrical shell: two numerical methods, *AIAA Journal* 4 (1966) 486–494.
[11] T.A. Smith, Numerical solution for the dynamic response of rotationally symmetric shells of revolution under transient loadings, US Army Missile Command Technical Report RS-TR-70-5, Redstone Arsenal, Alabama, 1970.
[12] T.A. Smith, Numerical analysis of rotationally symmetric shells under transient loadings, *AIAA Journal* 9 (1971) 637–643.
[13] T.A. Smith, Implicit high-order finite difference analysis of rotationally symmetric shells, US Army Missile Command Technical Report RL-73-9, Redstone Arsenal, Alabama, 1973.
[14] H. Radwan, J. Genin, Nonlinear modal equations for thin elastic shells, *International Journal of Non-linear Mechanics* 10 (1975) 15–29.
[15] T.A. Smith, Explicit high-order finite difference analysis of rotationally symmetric shells, US Army Missile Command Technical Report TL-77-1, Redstone Arsenal, Alabama, 1977.
[16] T.A. Smith, Explicit high-order finite difference analysis of rotationally symmetric shells, *AIAA Journal* 18 (1980) 309–317.
[17] Y.B. Chang, T.Y. Yang, W. Soedel, Linear dynamic analysis of revolutional shells using finite elements and modal expansion, *Journal of Sound and Vibration* 86 (1983) 523–538.
[18] T.A. Smith, Finite difference analysis of rotationally symmetric shells under discontinuous distributed loadings, US Army Missile Command Technical Report RL-83-5, Redstone Arsenal, Alabama, 1983.
[19] T.A. Smith, Finite difference analysis of rotationally symmetric shells under discontinuous distributed loadings, *AIAA Journal* 25 (1987) 1611–1621.
[20] T.A. Smith, Dynamic analysis of rotationally symmetric shells by the modal superposition method, US Army Missile Command Technical Report RD-ST-91-1, Redstone Arsenal, Alabama, 1991.

[21] T.A. Smith, Dynamic analysis of rotationally symmetric shells by the modal superposition method, *Journal of Sound and Vibration* 233 (2000) 515–543.
[22] T.A. Smith, Improved explicit high-order finite difference analysis of rotationally symmetric shells, US Army Missile Command Technical Report RD-ST-94-12, Redstone Arsenal, Alabama, 1994.
[23] T.A. Smith, Finite difference analysis of rotationally symmetric shells using variable node point spacings and incorporating matrix stability analysis, US Army Aviation and Missile Command Technical Report RD-PS-99-1, Redstone Arsenal, Alabama, 1998.
[24] T.A. Smith, Finite difference analysis of rotationally symmetric shells using variable node point spacings, *Journal of Sound and Vibration* 230 (2000) 1119–1145.
[25] W.R. Sellers Jr., A mathematical library for your PC, US Army Missile Command Letter Report No. AMSMI-RD-SS-88-25, Redstone Arsenal, Alabama, 1988.
[26] T.A. Smith, An evaluation of the accuracy of a numerical method for determining the eigenvalues and eigenvectors of a general matrix, US Army Aviation and Missile Command Technical Report RD-PS-02-03, Redstone Arsenal, Alabama, 2001.
[27] T.A. Smith, Matrix stability study for explicit numerical analysis of rotationally symmetric shells using eight first-order field equations, US Army Aviation and Missile Command Special Report RD-PS-02-02, Redstone Arsenal, Alabama, 2003.
[28] T.A. Smith, Explicit high-order finite difference analysis of rotationally symmetric shells using the displacement formulation of the equations and incorporating matrix stability analysis, US Army Research, Development, and Engineering Command Special Report AMR-PS-04-02, Redstone Arsenal, Alabama, 2004.
[29] E. Reissner, A new derivation of the equations for the deformation of elastic shells, *American Journal of Mathematics* 63 (1941) 177–184.